PAPER

Multi-material 4D printing to realize two-phase morphing in self-actuating structures

To cite this article: Hoo Min Lee *et al* 2024 *Smart Mater. Struct.* **33** 035007

IOP Publishing Smart Materials and Structures
Smart Mater. Struct. **33** (2024) 035007 (11pp) https://doi.org/10.1088/1361-665X/ad21b5

Multi-material 4D printing to realize two-phase morphing in self-actuating structures

Hoo Min Lee, Sol Ji Han, Min-Je Kim and Gil Ho Yoon*

Department of Mechanical Engineering, Hanyang University, Seoul 04763, Republic of Korea

E-mail: ghy@hanyang.ac.kr

Received 21 November 2023, revised 12 January 2024
Accepted for publication 23 January 2024
Published 2 February 2024

Abstract

4D printing has garnered significant attention within the field of engineering due to its capacity to introduce novel functionalities in printed structures through shape-morphing. Nevertheless, there persist challenges in the design and fabrication of intricate structures, primarily stemming from the intricate task of controlling variables that impact morphing characteristics. In order to surmount these hurdles, the approach of multi-material 4D printing is employed, underpinned by parametric studies, to actualize complex structures through a two-phase morphing process. This study specifically investigates the utilization of acrylonitrile butadiene styrene (ABS) and polycarbonate/ABS. The distinction in glass transition temperatures within these materials enables the realization of two distinct morphing phases. The research delves into the impact of structural parameters on morphing properties. Finite element analyses are subsequently conducted, leveraging the insights gained from parametric studies, to facilitate the accurate prediction of a diverse array of shape alterations in response to temperature fluctuations. Several structural models are both simulated and fabricated to experimentally validate the precise forecasting of desired morphing phases. The culmination of this study manifests in the design and fabrication of multiple multi-material structures, exemplifying both their functionality and intricate geometric complexity.

Keywords: multi-material 4D printing, two-phase morphing, thermal stimulation, glass transition temperature, self-actuating structure

1. Introduction

Initially, 4D printing was defined as the integration of 3D printing with the element of time, allowing the shape, property, or functionality of a 3D printed structure to change over time [1–3]. This field demonstrates remarkable capabilities including self-assembly, multi-functionality, and self-repair [4]. These features made 4D printing popular in various fields, and studies have been done to harness the potential of their applications. Research have been conducted on intelligent active hinges aimed at facilitating origami folding patterns [5], developing sequential self-folding structures [6], creating flexible electronic devices with shape memory polymers (SMPs) [7], and utilizing polylactic acid (PLA) to control electric currents [8]. Studies have also been conducted to investigate mechanisms of 4D printed composite spring [9], integrated sensor-actuator system with bio-inspired gradient gap [10], responsive structure using liquid-crystal polymeric materials [11], and photo switchable actuators with shape-switching behaviors [12]. The realm of meta-materials has also been explored, with studies focusing on energy absorption techniques employing smart sandwich structures [13, 14], the design of bio-mimetic

* Author to whom any correspondence should be addressed.

dome structures [15, 16], the manipulation of frequency bands using shape memory properties [17], the proposal of smart origami meta-materials [18], and the realization of multi-stable meta-materials with mechanically tunable performance [19].

Apart from its wide range of engineering applications, 4D printing has advantages in encompassing various 3D printing techniques, such as fused deposition modeling (FDM), stereolithography (SLA), selective laser sintering (SLS), and material jetting (MJ). FDM is a process that involves depositing thermo-plastic filaments layer by layer, while SLA is a process that uses photo-polymerization with lasers to solidify photo-curable resins, and SLS is a method of fusing powdered materials using lasers [20]. MJ is another 3D printing method where material is jetted onto a build platform using either a continuous or drop-on-demand approach [21]. Studies have been conducted using FDM to realize polyurethane-based SMPs with carbon nano-tubes [22], programmable shape memory 3D curved shell structures [23], and conductive SMP composites [24]. SLA has been employed to manufacture phase-switching structures [25], shape-recovering structures in hot water baths [26], and programmable shape-recovering structures under mechanical loading [27]. SLS was used in [28, 29] to fabricate magnetism-responsive grippers and self-healing structures. The MJ method was utilized in [30, 31] to demonstrate 4D printing of elastomer active hinges and present a novel 4D printed tunable frequency-selective surface utilizing a multi-layer mirror-stacked 'Miura-ori' structure.

For further enhancement of structural functionality in 4D printing, the concept of utilizing multi-materials has been explored across various engineering fields. Studies have sought to achieve diverse objectives, including the creation of 4D printed interlocking blocks through digital multi-material distribution [32, 33], the development of morphing wing flaps combining rigid components with flexible hinges [34], and the fabrication of functional bi-layers that combine highly hygroscopic active layers with hydrophobic restrictive and blocking layers [35]. Research efforts have also been directed towards the production of magnetic hydrogel-based soft actuators using multi-material direct ink printing [36], the proposal of bi-layer composite actuators for voltage control [37], and the realization of self-folding and self-opening structure through the utilization of multi-shape active composites [38]. Beyond the incorporation of multi-materials, the effect of programming concepts on shape memory functions have also been compared in [39]. Moreover, studies have delved into the integration of 4D printing with topology optimization and machine learning techniques to enhance functionalities. Topology optimization has been applied to determine the optimal distribution of material layouts in 4D printed active composites [40] and to optimize the structural design of porous poly-electrolyte soft actuators [41]. Machine learning has found applications in the development of soft pneumatic actuator robots [42], the design of active composite structures [43, 44], and the comprehensive understanding of the morphing responses with a unified data-driven approach [45].

Recently, mathematical modeling has assumed a pivotal role within the realm of 4D printing. Its importance has grown significantly, driven by the need to predict shape-shifting process, prevent collisions between components, and reduce the number of trial-and-error procedures [4]. Numerous studies have delved into the analysis of shape morphing by utilizing various mathematical models. For instance in [46], the influence of printing speed and structural thickness on the deformation behavior of shape memory PLA was investigated using the finite element method (FEM). In [47], the response surface method was harnessed to control torsional and flexural deformations in PLA plastic. Furthermore, comprehensive inquiries have been undertaken to elucidate the configuration of 4D printed composite laminates, employing FEM-based mathematical models [48]. Mathematical models accounting for thermodynamic visco-elastic properties have been explored in [49] to characterize the behavior of SMPs during the cooling and heating processes.

While many studies have sought to apply 4D printing in various engineering fields and enhance the functionality of 4D printed structures, relatively few have ventured into the utilization of mathematical modeling for realizing sequential deformations. In [50], mathematical modeling and experimental validation have been conducted for successfully predicting single phase permanent thermal deformations. Studies have been done on achieving sequential deformations using single materials with wide range of shape memory transition temperature ranges [51, 52] and considering multi-material approaches for self-folding [53]. The present study aims to step further by considering permanent sequential deformation and precisely controlling deformed geometry at distinct specific temperature ranges. Consequently, the objective of this study is to achieve two-phase morphing of multi-material structures and predict their morphing phases by utilizing FEM-based numerical analyses. This concept enables the design and fabrication of 4D printed structures that not only demonstrate functionality but also embody intricate geometric complexity.

This study employs acrylonitrile butadiene styrene (ABS) and polycarbonate/acrylonitrile butadiene styrene (PCABS), each characterized by specific glass transition temperatures of 105 °C and 125 °C, respectively. When subjected to their respective glass transition temperatures after 3D printing, reduction in structural length is observed due to the relaxation of internal tensile stresses. Structural bending is induced through variations in shrinkage lengths. The top layers and bottom layers are printed in longitudinal and lateral directions to achieve these differences. A series of experiments are conducted to explore the influence of structural dimensions, including length, width, and thickness, on the resulting curvatures after the morphing process. In addition to the experimental work, FEM-based simulations are carried out to assess the thermal material properties of ABS and PCABS. These simulations facilitate the prediction of the morphing processes for structures with intricate geometric complexity. Through transient thermal analysis, the distinct phases of structural deformation in response to temperature changes are observed. Leveraging the characterized material properties and insights

from the simulation of morphing phases, this study enables the modeling and fabrication of multi-material structures with complex geometric features. Such structures include a self-actuating chair, a stent with varying thickness, and an exoskeleton suit. Notably, these structures successfully achieve the desired geometries following a two-phase thermal stimulation, affirming the viability of the proposed multi-material 4D printing approach for the realization of designs with unprecedented complexity.

2. Theory

Semi-crystalline polymers undergo reversible transitions from relatively hard and brittle glassy states to viscous rubbery states when heated or cooled within specific glass transition temperature T_g. This mechanism allows the achievement of shape memory effect (SME) and shape change. The SME is realized when the recovery of the original shape is achieved through heating above T_g, with either chemical or physical cross-links storing elastic energy during the programming stage and serving as the driving force for recovery in the later stages [54]. The present research focuses on permanent shape change of semi-crystalline polymers. During the 3D printing process, which involves the extrusion of thick filaments through narrow nozzles, significant tensile stress is induced along the length direction. This results in highly oriented residual stress, which refers to stresses retained within the material even after the original cause of the stresses has been removed [55]. The relaxation of this internal stress causes the printed filament to return to its original geometry, as it was before being compressed in the nozzle, leading to a reduction in the length of the printed specimen. In the case of semi-crystalline polymers, this stress relaxation is achieved by heating the material to its specific glass transition temperature T_g. The deformation process is illustrated in figure 1.

Using the concept of reducing the length of printed filament by applying thermal stimulation, various structural deformation can be realized by adjusting the printing angles. For homogeneous rectangular bars illustrated in figures 2(a) and (b), high volume shrinkage in longitudinal direction and relatively lower volume shrinkage in lateral direction are realized when printed in their respective orientations. Using these differences in shrinkage volumes, structural bending can be realized. This is demonstrated in figure 2(c), where a composite rectangular bar bends upwards when the top half layers are printed in the longitudinal direction while the remaining bottom layers are printed in the lateral direction.

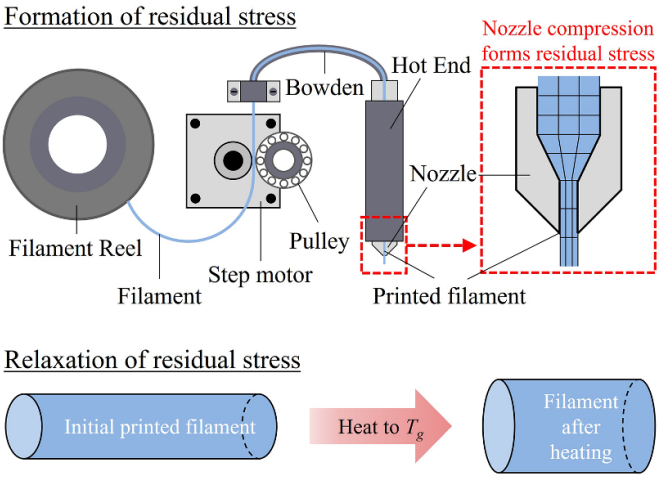

Figure 1. Using thermal stimulation to deform printed filament by relieving residual stress at glass transition temperature.

3. Materials and methods

3.1. Materials

The present study adopts the concept of achieving structural bending through thermal stimulation. ABS and PCABS (60% PC and 40% ABS) are employed as the semi-crystalline polymers to facilitate a two-phase shape morphing process at respective T_g values. Based on the experimental investigations using DNA analysis in [56], ABS and PCABS have T_g values of 105 °C and 125 °C, respectively. ABS is chosen over other 3D printing materials due to its high shrinkage rate, making it suitable to realize structural morphing involving large deformations. PCABS is a material manufactured based on ABS, with similar thermal deformation characteristics but relatively higher thermal resistance. Thus, two-phase morphing can be achieved, and the deformed geometry can be controlled by utilizing the two materials. The components required for structural bending are printed in longitudinal and lateral orientations. For the remaining components, method of utilizing raster angles is employed to change the direction of shape change [57–59]. These parts are printed at a 45° angle in the transverse direction to suppress both volume shrinkage and structural bending.

The degree of structural bending depends on the shrinkage volume when thermally stimulated, and it is influenced by the thermal expansion coefficient. Since coefficient values exhibit a significant decrease at glass transition temperatures [60], accurately assessing these changes is crucial for predicting changes in structural geometry during morphing phases. Therefore, both experimental studies and numerical analyses are conducted to evaluate the thermal expansion coefficients of ABS and PCABS at various temperature values. Initially, experiments are carried out on structures with different parameters to achieve morphed geometry with varying curvatures. Subsequently, numerical analyses are performed to correlate the experimental and simulated curvature values and evaluate the thermal expansion coefficients of ABS and PCABS.

3.2. Experimental method

A series of experiments is carried out to examine the effects of structural length l, width w, and thickness t on the resulting curvatures after the morphing process. A H-beam structure is employed for experimental characterization of the parameters,

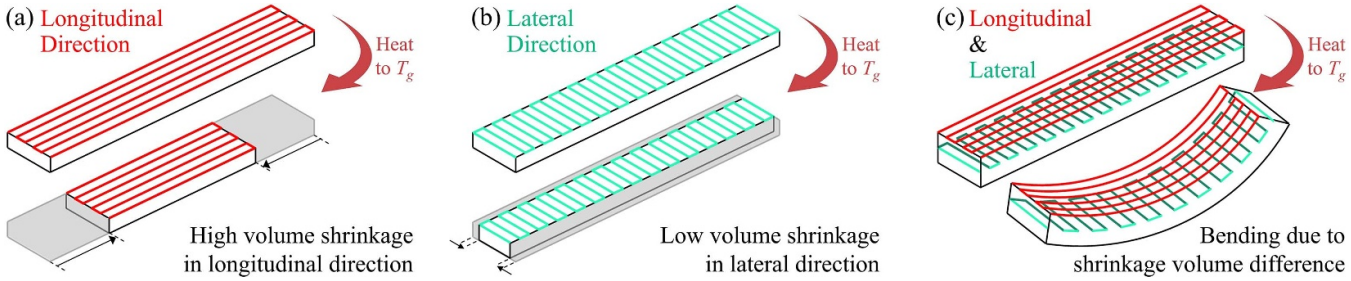

Figure 2. Realization of varying structural deformation at different printing angles: (a) shrinkage in longitudinal direction, (b) shrinkage in lateral direction, and (c) structural bending due to shrinkage volume difference.

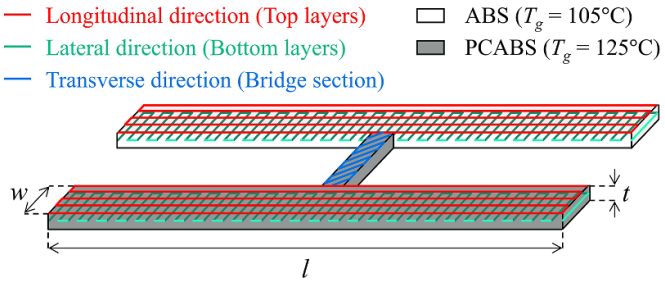

Figure 3. Schematic of H-beam structure to conduct experimental characterization of structural parameters.

and its schematic is provided in figure 3. This structure consists of two rectangular bi-layer composites, with the top half layers printed longitudinally and the remaining bottom layers printed laterally. One of these composites is printed using ABS, while the other is printed using PCABS. Both composites are interconnected by a bridge section, a homogeneous rectangular PCABS structure uniformly printed in a 45° transverse orientation. Each bi-layer composite within the reference H-beam structure is fabricated with $l = 80$ mm, $w = 5$ mm, and $t = 2.0$ mm. To assess the effects of parameters on curvatures, structures with different parameters are compared to the reference structure. Structures with $l = 40$ mm, 60 mm, 100 mm, and 120 mm are fabricated to evaluate length effects. For assessing width effects, structures with $w = 5.0$ mm, 7.5 mm, 12.5 mm, and 15.0 mm are used. The evaluation of thickness effects includes structures with $t = 1.0$ mm, 1.5 mm, 2.5 mm, and 3.0 mm. Parameters not under comparison are kept identical to those of the reference structure.

The structure is fabricated using a Flashforge creator 3 Pro printer equipped with dual nozzles. The printing speed is set as 30 mm s^{-1} to ensure a sufficient time period between extrusion and deposition of each layer during the process. This is done to prevent the printing speed from becoming a factor affecting thermal expansion rate, as observed in the variation of residual strain due to the time taken for layer deposition in [61]. Extruder temperatures are set as 230 °C and 248 °C for ABS and PCABS, respectively. The platform temperature is set as 90 °C. These temperatures values are chosen to ensure platform adhesion and prevent unwanted excessive shrinkage during the extrusion process, thus improving the printing quality. The Flashforge ABS and PCA11705-BLK PCABS filaments of 1.75 mm diameter are extruded through nozzles of 0.40 mm to print layers with thickness of 0.25 mm. Application of thermal stimulation is done by placing the fabricated structure in an oven and setting the temperature to 160 °C. The CSIR-10 thermal imaging camera measures the structural temperature to precisely observe the points at which the morphing phases begin. A total of 10 experiments are conducted for each case, and the average results are used to evaluate the curvatures after morphing. The variance values are also calculated for each case to assess the reliability of the average curvature values.

3.3. Numerical analysis

Numerical analysis is conducted to assess the varying thermal expansion coefficients of ABS and PCABS over temperature variation. Transient thermal analysis is performed using ANSYS 2021/R2 Workbench to account for the time-dependent distribution of structural temperatures before reaching a steady state. The structures subjected to the simulation are discretized using 3D 20-node solid elements to exhibit quadratic displacement behaviors. Additionally, the large deflection option is considered to account for nonlinear large deformations observed during the morphing phases. The material properties data compiled by ANSYS GRANTA are utilized, and the corresponding values are detailed in table 1. The convection film coefficient, ambient temperature, and analysis time period were set as 15 $Wm^{-2}K^{-1}$, 160 °C, and 150 s, respectively. The curvatures of end results for each case are compared with the experimental curvatures to acquire the thermal expansion coefficient values.

4. Results and discussion

The experiment successfully demonstrated two-phase sequential morphing within the H-beam structure. The first and second morphing phases are illustrated in figures 4(a) and (b), where the ABS and PCABS components deformed in a sequential manner at structural temperatures of 105 °C and 125 °C, respectively. It is noteworthy that the ABS component did not deform additionally during the second morphing phase as the residual stress was completely relieved in the initial morphing phase.

Table 1. Material properties for transient thermal analysis.

Acrylonitrile butadiene styrene (ABS)						
Young's modulus	Bulk modulus	Shear modulus	Poisson's ratio	Density	Thermal conductivity	Specific heat capacity
2408 MPa	4352.9 MPa	855.24 MPa	0.4078	1050 kg m^{-3}	0.2301 Wm^{-1} K^{-1}	1400 Jkg^{-1} K^{-1}
Polycarbonate/acrylonitrile butadiene styrene (PCABS)						
Young's modulus	Bulk modulus	Shear modulus	Poisson's ratio	Density	Thermal conductivity	Specific heat capacity
2513 MPa	4086.2 MPa	899.11 MPa	0.3975	1109 kg m^{-3}	0.2670 Wm^{-1} K^{-1}	1449 Jkg^{-1} K^{-1}

(a) (b)

Figure 4. Structural bending of the reference H-beam structure: (a) at 105 °C and (b) at 125 °C.

It could also be observed that structures with different parameters morphed to have different curvatures. The deformed structures are shown in figure 5. The curvature κ was calculated using the measured values of arc width b and arc height h of the morphed structure, using the following formulation:

$$\kappa = \frac{8h}{b^2 + 4h^2} \tag{1}$$

The reference structure exhibited average curvatures of 0.0189 mm^{-1} and 0.0258 mm^{-1} for ABS and PCABS components, respectively. The variance values for the average curvatures were evaluated as 2.33×10^{-6} mm^{-2} and 9.46×10^{-6} mm^{-2}, respectively. Structures with different parameters produced different curvature values, as presented in table 2. The results show that structural length l does not affect the degree of structural bending as the curvature values show consistency despite variations in the l values. However, different results are derived for width w and thickness t, where their increased values led to decrease in curvatures of both composites. Specifically, the curvatures of ABS and PCABS composites decreased by average 0.0071 mm^{-1} and 0.0118 mm^{-1} respectively, as w increased from 5 mm to 15 mm. The curvatures of ABS and PCABS composites decreased by average 0.0640 mm^{-1} and 0.1079 mm^{-1}, respectively, when t was increased from 1 mm to 3 mm. Notably, PCABS composites exhibited greater changes in curvature values compared to ABS composites under identical parameter variations.

The numerical analysis allowed the realization of structural bending during morphing phases, as a result of shrinkage volume difference between layers printed longitudinally and laterally. The analysis aimed to coordinate the experimental and simulated curvature values for structures with varying t values, as the curvatures exhibited the most pronounced nonlinear changes with variations in this parameter. This process facilitated the evaluation of the thermal

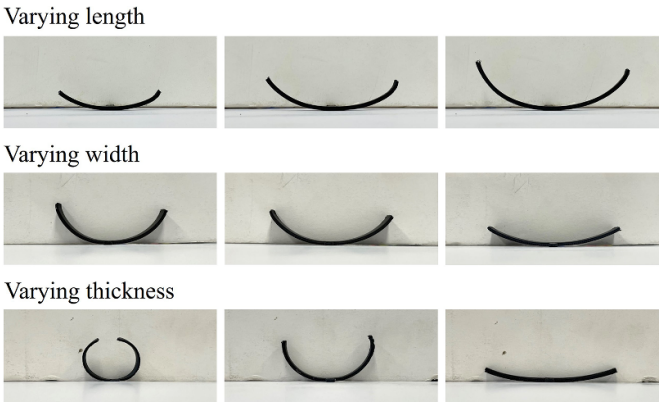

Figure 5. Deformed structures with various curvatures. PCABS components are presented for clear visualization.

expansion coefficients of ABS and PCABS, and the results are presented in figure 6. Both materials demonstrate a tendency of decreasing coefficient values in response to increasing temperature. Furthermore, it is worth noting that these values exhibit a sharp decrease in the respective glass transition temperature regions that are highlighted in the graph.

The assessed coefficients were also utilized to conduct analyses on structures with varying length and width. The simulated results of curvature values are presented in table 3, and illustrations of the simulated structural deformations are shown in figure 7. The assessed coefficients resulted in great coordination between experimental and simulated curvature values for all cases, with most cases exhibiting error percentages near or below 10%. The only exception is the ABS structure with a length of 40.0 mm, showing an error percentage of 14.67%. The disparity between the experimental and numerical results stems from the inconsistency in curvature values throughout the structure, which is most noticeable when comparing the bottom-left structures in figures 5 and 7. The inconsistent curvature values of the experimental morphed structures resulted from slight deformations at the ends of the structure. This phenomenon occurred due to the effect of gravity and the decrease in elastic modulus with increased structural temperature, as discussed in [57]. This explains the exceptional case, which had a relatively higher error percentage compared to other cases, as its involvement with the structure of the smallest length led to a relatively greater error in curvature calculation using equation (1). Despite

Table 2. Experimental results of different curvatures with variation of structural parameters.

Parameter		Structure with varying length				Structure with varying width				Structure with varying thickness			
Length (mm)		40.0	60.0	100.0	120.0	80.0				80.0			
Width (mm)		5.0				7.5	10.0	12.5	15.0	5.0			
Thickness (mm)		2.0				2.0				1.0	1.5	2.5	3.0
ABS curvature	Average (mm^{-1})	0.0184	0.0190	0.0188	0.0183	0.0167	0.0147	0.0132	0.0118	0.0708	0.0330	0.0129	0.0068
	Variance ($\times 10^{-6}$ mm^{-2})	13.51	9.19	4.43	10.00	12.76	6.46	7.75	4.70	16.23	10.74	1.29	1.78
PCABS curvature	Average (mm^{-1})	0.0256	0.0263	0.0249	0.0254	0.0209	0.0162	0.0134	0.0109	0.1129	0.0500	0.0121	0.0050
	Variance ($\times 10^{-6}$ mm^{-2})	3.39	3.25	6.10	11.10	6.99	14.14	11.52	8.62	12.15	4.13	6.45	1.82

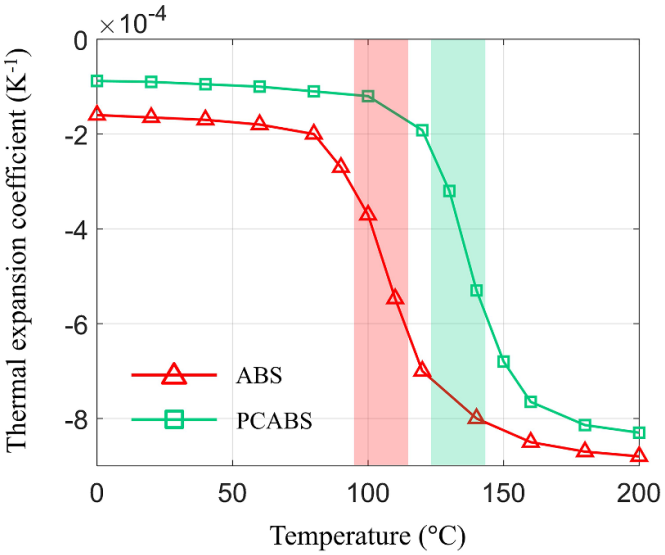

Figure 6. Changes in thermal expansion coefficient values over temperature variation. These values were evaluated by coordinating the average curvature values of deformed specimens with curvatures of simulated structures.

some disparity between the experimental and simulated results, error percentages within 10% indicate that the nonlinear large deformation behavior is well realized in the simulated structure, enabling accurate prediction of the morphing phases at different temperatures.

5. Case studies

We apply our approach to manufacture several self-actuating multi-material structures through three case studies, each involving structure modeling, numerical analysis, and experimental validation. The numerical analysis utilized the simulation process outlined in section 4, incorporating the thermal expansion coefficients evaluated in figure 6. Experimental validation involved heating the structures in the oven set to reach 160°C, while the CSIR-10 thermal imaging camera monitored the structure temperature. Each case study was explicitly conducted to verify the functionality and practicality of the proposed multi-material methodology.

In the first case study, we aim to demonstrate that sequential morphing can be achieved in structures presenting greater geometric challenges than H-beam structures. We consider a self-actuating chair that transforms from a 2D state to a 3D configuration, where the leg and headrest components morph sequentially. The structure is modeled as shown in figure 8(a). To induce downward bending of the chair legs in the first phase, the bottom five layers and the next five layers are printed using ABS in longitudinal and lateral directions, respectively. Five additional PCABS layers are stacked to reinforce the chair legs, ensuring their ability to support the chair body during the initial morphing phase. The headrest component comprises ten PCABS layers, with the bottom five and top five layers printed laterally and longitudinally, respectively, to induce upward bending in the following morphing phase. The remaining components are designed as homogeneous PCABS structures with layers printed at a 45° orientation. All layers in the structure have a thickness of 0.25 mm. Numerical analysis and experimental validation were conducted based on the modeled structure. The simulated and actual morphing phases are illustrated in figure 8(b). For the simulated model, the curvature values of leg and headrest were evaluated as 0.0519 mm^{-1} and 0.0315 mm^{-1}, respectively. A great coordination between the simulated model and the actual structure was observed, with the experimental curvature values having differences of 7.21% and 9.43% for the leg and headrest, respectively. Moreover, both the model and the structure successfully demonstrated sequential morphing with a smooth transition around 125 seconds after applying thermal stimulation. This case study confirms that sequential two-phase morphing can be achieved in structures beyond simple H-beam structures.

In the next case study, we aim to conduct precise modeling to successfully induce sequential morphing phases and prevent interruptions between them. We consider a self-actuating stent designed to transform from a 2D state to a 3D configuration

Table 3. Simulated results of different curvatures with variation of structural parameters.

Parameter	Structure with varying length				Structure with varying width				Structure with varying thickness			
Length (mm)	40.0	60.0	100.0	120.0	80.0				80.0			
Width (mm)	5.0				7.5	10.0	12.5	15.0	5.0			
Thickness (mm)	2.0				2.0				1.0	1.5	2.5	3.0
ABS curvature (mm^{-1})	0.0211	0.0202	0.0200	0.0200	0.0174	0.0150	0.0134	0.0123	0.0625	0.0342	0.0121	0.0068
PCABS curvature (mm^{-1})	0.0284	0.0280	0.0277	0.0276	0.0205	0.0160	0.0133	0.0115	0.1093	0.0548	0.0129	0.0049

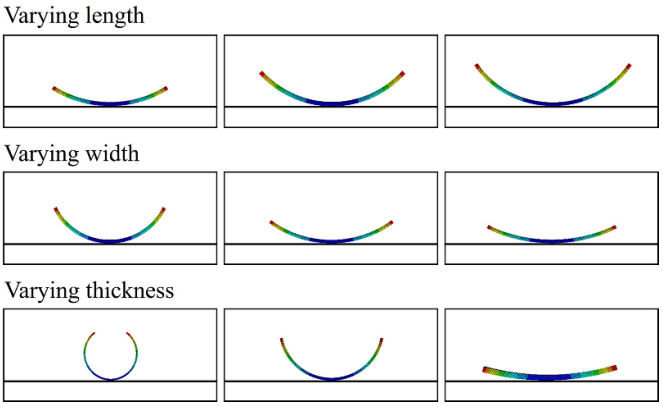

Figure 7. Simulated structures with various curvatures. PCABS components are presented for comparison with figure 5(b).

with varying cross-sectional areas. The structure is modeled as illustrated in figure 9(a). To morph the structure into a pipe-like geometry during the initial phase, the components along the lateral direction are modeled using ABS, with the bottom four and top four layers printed in the lateral and longitudinal directions, respectively. The remaining components along the longitudinal direction are modeled using PCABS to induce varying cross-sectional areas in the following phase. These components consist of four layers, with half printed in the longitudinal direction and the other half in the lateral direction. All layers have a thickness of 0.25 mm. Numerical analysis and experimental validation were conducted for the proposed model. The simulated morphing phases are shown in figure 9(b). The curvature values of ABS and PCABS components were evaluated as 0.0719 mm^{-1} and 0.0217 mm^{-1}, respectively. Experimental validation was performed on the model, and the manufactured structure at different phases is presented in figure 9(b). The manufactured structure exhibited great coordination with the simulated model, with the experimental curvature values having maximum differences of 2.35% and 5.60% for the ABS and PCABS components, respectively. Additionally, we have observed cases where the two morphing phases interrupted each other, resulting in undesired structures, as shown in figure 9(c). This anomaly occurred when the thickness values of PCABS components were set smaller than those of the modeled structure, reducing the time required for these components to reach their glass transition temperatures. Consequently, the second morphing phase was triggered around 50 seconds after applying thermal stimulation, before the expected end time of the initial morphing phase at 83 seconds. This case study demonstrates that the key to successful sequential morphing lies in precise modeling and necessitates careful consideration of material thickness and convection conditions to prevent materials from reaching glass transition temperatures simultaneously.

For the final case study, our objective is to control the curvatures of different components to achieve the desired geometry after the morphing phases. We consider a wearable lower limb exoskeleton, which includes a shoe sole, toe cap, shoe straps, curved heel bar, calf supporter, and calf straps. An example of the wearable exoskeleton is presented in figure 10(a). Precise modeling is done to determine the appropriate structural thicknesses for controlling the bending degrees of the toe cap, heel bar, shoe straps and calf straps. Similar to the case of fabricating a shoe supporter done previously in [62], where separately printed components were combined, our case study aims to go further by realizing the exoskeleton in a single printing process. The structure is modeled as shown in figure 10(b). ABS is employed for the toe cap and heel bar to induce bending in the first morphing phase. The toe cap consists of a total of five layers, with the top two layers printed longitudinally, the next two layers printed laterally, and the bottom layer printed using PCABS in the lateral orientation to prevent excessive bending. The heel bar consists of two parts that bend in opposite directions, forming an S-shape to fit securely around the heel and ankle area. The part that bends upwards is composed of the top four ABS layers printed longitudinally, the middle two ABS layers printed laterally, and the bottom two PCABS layers printed laterally. The remaining part comprises the bottom four ABS layers printed longitudinally, the middle three ABS layers printed laterally, and the top PCABS layer printed laterally. The shoe and calf straps are entirely modeled using PCABS to induce bending in the second morphing phase. The exoskeleton includes four pairs of shoe straps, each varying in bending behavior. The first pair, nearest to the toe cap, consists

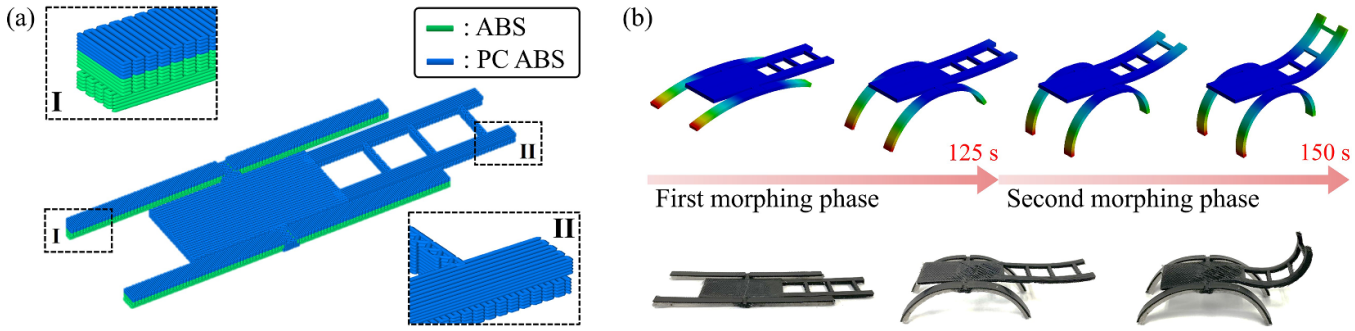

Figure 8. Case study 1. (a) 3D sliced view of the self-actuating chair and (b) the morphing phases when applied with thermal stimulation.

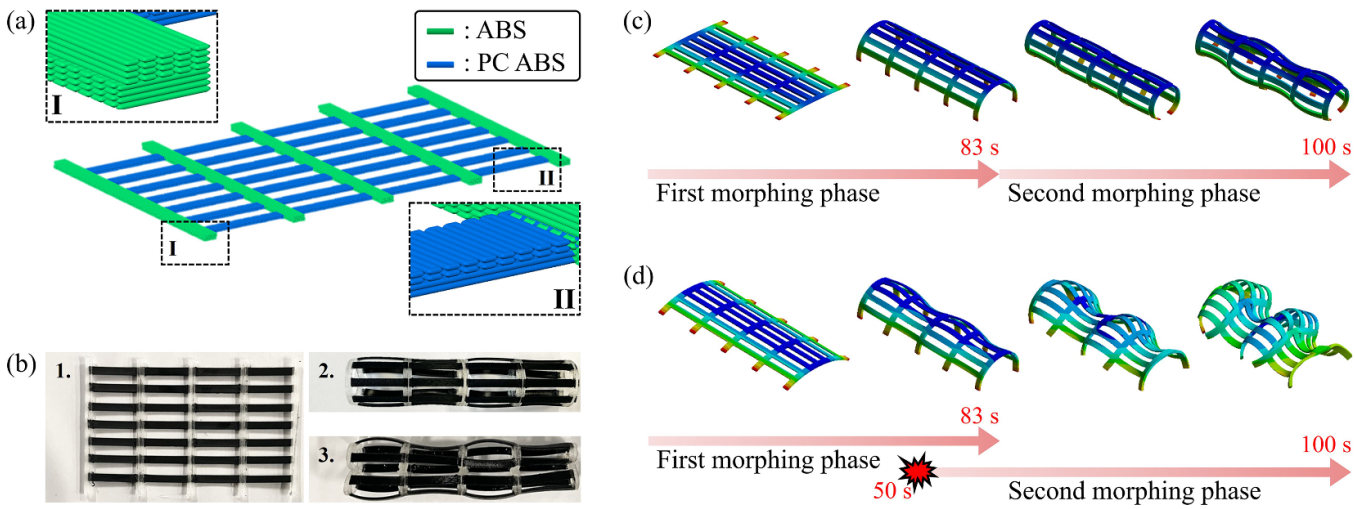

Figure 9. Case study 2. (a) 3D sliced view of the self-actuating stent, (b) fabricated and realized stent: 1.Initial printed state 2. Geometry after first morphing phase 3. Geometry after second morphing phase, (c) simulated case with successful sequential morphing, and (d) simulated case with interrupted morphing.

of three layers, with the top layer printed longitudinally and the bottom two layers laterally. Subsequent pairs, progressing sequentially from the front, comprise a total of four, six, and eight layers, respectively, to achieve varying degrees of bending. For the calf strap, five pairs are included in the exoskeleton, designed to make the pair closest to the heel bar bend the most, with the straps above bending to a lesser degree. All these straps have an equal number of longitudinal and lateral layers. The first pair, closest to the heel bar, comprises six layers, while the following two pairs each comprise eight layers, and the remaining two pairs consist of ten layers, enabling different degrees of bending. All layers have a thickness of 0.25 mm.

Numerical analysis and experimental validation were conducted for the proposed exoskeleton design. Illustrations of the simulated and experimental morphing phases are shown in figures 10(c) and (d). For the simulated model, the toe cap, heel bar sections with upward and downward bending were evaluated to have curvatures of 0.0809 mm^{-1}, 0.0489 mm^{-1}, and 0.0514 mm^{-1}, respectively. For the shoe straps, starting from the first pair nearest to the toe cap in sequential order, they were evaluated to have curvatures of 0.1103 mm^{-1}, 0.1017 mm^{-1}, 0.0791 mm^{-1}, and 0.0590 mm^{-1}, respectively. For the calf straps, starting from the first pair closest to the heel bar in sequential order, they had curvatures of 0.0859 mm^{-1}, 0.0517 mm^{-1}, 0.0517 mm^{-1}, 0.0338 mm^{-1}, and 0.0338 mm^{-1}, respectively. A great coordination between the simulated model and the manufactured structure was observed, with the experimental curvatures having differences within 8% range overall. Moreover, both the model and the structure presented smooth transition in morphing phases at approximate time period of 96 seconds after applying thermal stimulation. The three case studies successfully demonstrate the feasibility of the proposed multi-material 4D printing

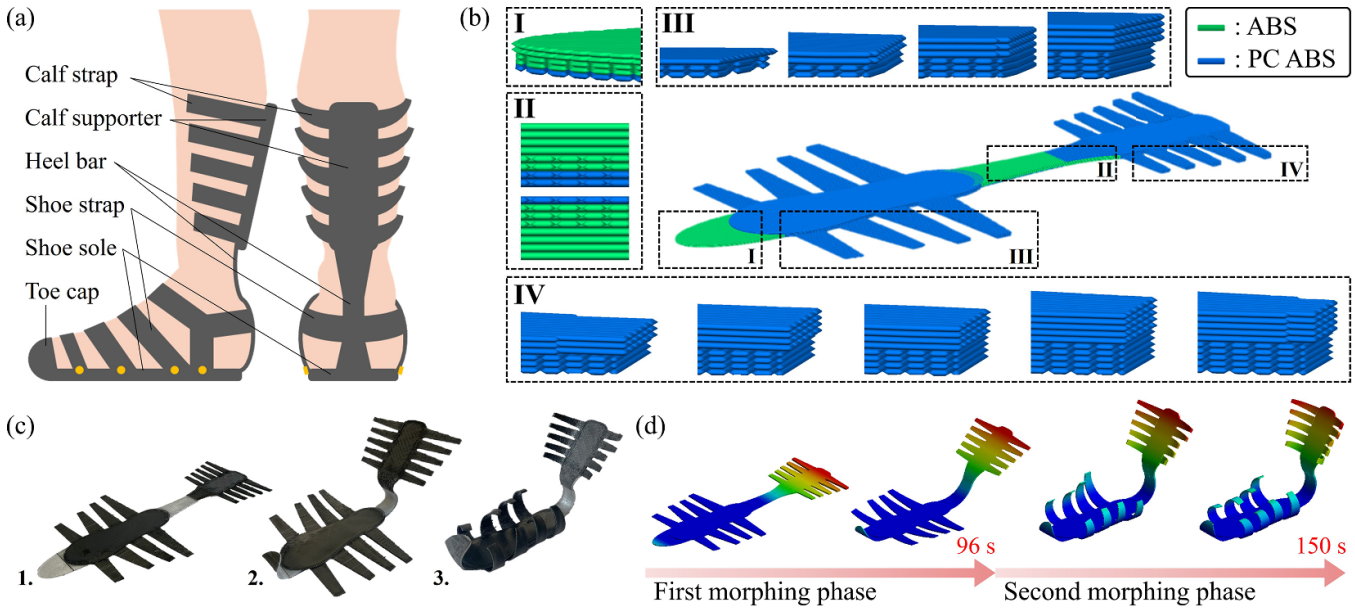

Figure 10. Case study 3. (a) Example of a wearable lower limb exoskeleton, (b) 3D sliced view of the exoskeleton, (c) fabricated and realized exoskeleton: 1. Initial printed state 2. Geometry after first morphing phase 3. Geometry after second morphing phase, and (d) morphing phases of the self-actuating wearable exoskeleton.

method for fabricating and realizing self-actuating structures with intricate geometric complexity.

6. Conclusions

This study proposed a multi-material 4D printing approach to achieve a two-phase morphing in structures with complex designs. ABS and PCABS plastics were considered to initiate morphing at their glass transition temperatures, specifically 105 °C and 125 °C. For the morphing process, structures were printed with longitudinal orientations for the top half layers and lateral orientations for the bottom layers, enabling structural bending during the morphing phases. Parameter characterization was conducted to explore the influence of structural length, width, and thickness on the degree of curvature after morphing. Experiments using specimens with various parameter values were conducted, and the results were employed in FEM analyses involving transient heat convection simulations, to evaluate the thermal expansion coefficients of ABS and PCABS at different temperatures. This meticulous process enabled the precise assessment of morphing phases at different temperatures. Multi-material structures such as self-actuating chair, stent, and exoskeleton suit were modeled and manufactured for validation. The study concludes with the design and production of these multi-material structures, which showcase not only functionality but also intricate geometric complexity.

Data availability statement

The data cannot be made publicly available upon publication because they are not available in a format that is sufficiently accessible or reusable by other researchers. The data that support the findings of this study are available upon reasonable request from the authors.

Acknowledgments

This research was supported by the National Research Foundation of Korea (NRF) grant funded by the Korea government (MSIT) (NRF-2019R1A2C2084974).

Conflict of interest

The author(s) declare no conflicts of interest with respect to the research, authorship, and/or publication of this article.

ORCID iDs

Hoo Min Lee https://orcid.org/0000-0002-6049-7149
Gil Ho Yoon https://orcid.org/0000-0002-0634-8329

References

[1] Tibbits S 2014 4D printing: multi-material shape change *Archit. Des.* **84** 116–21
[2] Ge Q, Qi H J and Dunn M L 2013 Active materials by four-dimension printing *Appl. Phys. Lett.* **103** 131901
[3] Khoo Z X, Teoh J E M, Liu Y, Chua C K, Yang S, An J, Leong K F and Yeong W Y 2015 3D printing of smart materials: a review on recent progresses in 4D printing *Virtual Phys. Prototyp.* **10** 103–22
[4] Momeni F, Liu X, Ni J and Ni J 2017 A review of 4D printing *Mater. Des.* **122** 42–79
[5] Ge Q, Dunn C K, Qi H J and Dunn M L 2014 Active origami by 4D printing *Smart Mater. Struct.* **23** 094007
[6] Mao Y, Yu K, Isakov M S, Wu J, Dunn M L and Jerry Qi H 2015 Sequential self-folding structures by 3D printed digital shape memory polymers *Sci. Rep.* **5** 1–12
[7] Zarek M, Layani M, Cooperstein I, Sachyani E, Cohn D and Magdassi S 2016 3D printing of shape memory polymers for flexible electronic devices *Adv. Mater.* **28** 4449–54

[8] Mitkus R, Cerbe F and Sinapius M 2022 4D printing electro-induced shape memory polymers *Smart Materials in Additive Manufacturing, Volume 2: 4D Printing Mechanics, Modeling and Advanced Engineering Applications* (Elsevier) pp 19–51

[9] Van Hoa S 2019 Development of composite springs using 4D printing method *Compos. Struct.* **210** 869–76

[10] Chen D *et al* 2020 4D printing strain self-sensing and temperature self-sensing integrated sensor-actuator with bioinspired gradient gaps *Adv. Sci.* **7** 2000584

[11] López-Valdeolivas M, Liu D, Broer D J and Sánchez-Somolinos C 2018 4D printed actuators with soft-robotic functions *Macromol. Rapid Commun.* **39** 1700710

[12] Lu X, Ambulo C P, Wang S, Rivera-Tarazona L K, Kim H, Searles K and Ware T H 2021 4D-printing of photoswitchable actuators *Angew. Chem., Int. ed.* **60** 5536–43

[13] Serjouei A, Yousefi A, Jenaki A, Bodaghi M and Mehrpouya M 2022 4D printed shape memory sandwich structures: experimental analysis and numerical modeling *Smart Mater. Struct.* **31** 055014

[14] Bodaghi M, Serjouei A, Zolfagharian A, Fotouhi M, Rahman H and Durand D 2020 Reversible energy absorbing meta-sandwiches by FDM 4D printing *Int. J. Mech. Sci.* **173** 105451

[15] Tezerjani S M D, Yazdi M S and Hosseinzadeh M H 2022 The effect of 3D printing parameters on the shape memory properties of 4D printed polylactic acid circular disks: an experimental investigation and parameters optimization *Mater. Today Commun.* **33** 104262

[16] Li G *et al* 2023 Biomimetic 4D printing of dome-shaped dynamic mechanical metamaterials *J. Mater. Res. Technol.* **24** 4047–59

[17] Li B, Zhang C, Peng F, Wang W, Vogt B D and Tan K 2021 4D printed shape memory metamaterial for vibration bandgap switching and active elastic-wave guiding *J. Mater. Chem.* C **9** 1164–73

[18] Tao R, Ji L, Li Y, Wan Z, Hu W, Wu W, Liao B, Ma L and Fang D 2020 4D printed origami metamaterials with tunable compression twist behavior and stress-strain curves *Composites* B **201** 108344

[19] Tao R, Xi L, Wu W, Li Y, Liao B, Liu L, Leng J and Fang D 2020 4D printed multi-stable metamaterials with mechanically tunable performance *Compos. Struct.* **252** 112663

[20] Kafle A, Luis E, Silwal R, Pan H M, Shrestha P L and Bastola A K 2021 3D/4D Printing of polymers: Fused deposition modelling (FDM), selective laser sintering (SLS) and stereolithography (SLA) *Polymers* **13** 3101

[21] Rafiee M, Farahani R D and Therriault D 2020 Multi-material 3D and 4D printing: a survey *Adv. Sci.* **7** 1902307

[22] Ly S T and Kim J Y 2017 4D printing–fused deposition modeling printing with thermal-responsive shape memory polymers *Int. J. Prec. Eng. Manufac.-Green Technol.* **4** 267–72

[23] Hu G, Damanpack A, Bodaghi M and Liao W H 2017 Increasing dimension of structures by 4D printing shape memory polymers via fused deposition modeling *Smart Mater. Struct.* **26** 125023

[24] Nguyen T T and Kim J 2020 4D-printing-Fused deposition modeling printing and PolyJet printing with shape memory polymers composite *Fibers Polymers* **21** 2364–72

[25] Choong Y Y C, Maleksaeedi S, Eng H, Wei J and Su P-C 2017 4D printing of high performance shape memory polymer using stereolithography *Mater. Des.* **126** 219–25

[26] Zhao T, Yu R, Li X, Cheng B, Zhang Y, Yang X, Zhao X, Zhao Y and Huang W 2018 4D printing of shape memory polyurethane via stereolithography *Eur. Polymer J.* **101** 120–6

[27] Zhao J, Han M and Li L 2021 Modeling and characterization of shape memory properties and decays for 4D printed parts using stereolithography *Mater. Des.* **203** 109617

[28] Wu H, Wang O, Tian Y, Wang M, Su B, Yan C, Zhou K and Shi Y 2020 Selective laser sintering-based 4D printing of magnetism-responsive grippers *ACS Appl. Mater. Interfaces* **13** 12679–88

[29] Ouyang H, Li X, Lu X and Xia H 2022 Selective laser sintering 4D printing of dynamic cross-linked polyurethane containing diels–alder bonds *ACS Appl. Polymer Mater.* **4** 4035–46

[30] Moore J P and Williams C B 2015 Fatigue properties of parts printed by PolyJet material jetting *Rapid Prototyp. J.* **21** 675–85

[31] Cui Y, Nauroze S A, Bahr R and Tentzeris M M 2021 A novel additively 4D printed origami-inspired tunable multi-layer frequency selective surface for mm-Wave IoT, RFID, WSN, 5G and smart city applications *2021 IEEE MTT-S Int. Microwave Symp. (IMS)* (IEEE) pp 86–89

[32] Benyahia K, Seriket H, Prod'hon R, Gomes S, André J C, Qi H J and Demoly F 2022 A computational design approach for multi-material 4D printing based on interlocking blocks assembly *Addit. Manuf.* **58** 102993

[33] Benyahia K, Seriket H, Prod'hon R, Gomes S, André J C, Qi H J and Demoly F 2023 Design for multi-material 4D printing: Development of an algorithm for interlocking blocks assembly generation *Proc. CIRP* **119** 396–401

[34] Akbari S, Sakhaei A H, Kowsari K, Yang B, Serjouei A, Yuanfang Z and Ge Q 2018 Enhanced multimaterial 4D printing with active hinges *Smart Mater. Struct.* **27** 065027

[35] Tahouni Y, Krüger F, Poppinga S, Wood D, Pfaff M, Rühe J, Speck T and Menges A 2021 Programming sequential motion steps in 4D-printed hygromorphs by architected mesostructure and differential hygro-responsiveness *Bioinsp. Biomim.* **16** 055002

[36] Simińska-Stanny J, Nizioł M, Szymczyk-Ziółkowska P, Brożyna M, Junka A, Shavandi A and Podstawczyk D 2022 4D printing of patterned multimaterial magnetic hydrogel actuators *Addit. Manuf.* **49** 102506

[37] Wang Y and Li X 2021 4D printing reversible actuator with strain self-sensing function via structural design *Composites* B **211** 108644

[38] Wu J, Yuan C, Ding Z, Isakov M, Mao Y, Wang T, Dunn M L and Qi H J 2016 Multi-shape active composites by 3D printing of digital shape memory polymers *Sci. Rep.* **6** 24224

[39] Samal B B, Jena A, Varshney S K and Siva K C 2023 4D printing of shape memory polymers: a comparative study of programming methodologies on various material properties *Smart Mater. Struct.* **32** 074003

[40] Athinarayanarao D, Prod'hon R, Chamoret D, Qi H J, Bodaghi M, André J C and Demoly F 2023 Computational design for 4D printing of topology optimized multi-material active composites *npj Comput. Mater.* **9** 1

[41] Zolfagharian A, Denk M, Bodaghi M, Kouzani A Z and Kaynak A 2020 Topology-optimized 4D printing of a soft actuator *Acta Mech. Solida Sinica* **33** 418–30

[42] Zolfagharian A, Durran L, Gharaie S, Rolfe B, Kaynak A and Bodaghi M 2021 4D printing soft robots guided by machine learning and finite element models *Sens. Actuators* A **328** 112774

[43] Hamel C M, Roach D J, Long K N, Demoly F, Dunn M L and Qi H J 2019 Machine-learning based design of active composite structures for 4D printing *Smart Mater. Struct.* **28** 065005

[44] Sun X, Yue L, Yu L, Shao H, Peng X, Zhou K, Demoly F, Zhao R and Qi H J 2022 Machine learning-evolutionary

algorithm enabled design for 4D-printed active composite structures *Adv. Funct. Mater.* **32** 2109805
[45] Su J W, Li D, Xie Y, Zhou T, Gao W, Deng H, Xin M and Lin J 2020 A machine learning workflow for 4D printing: understand and predict morphing behaviors of printed active structures *Smart Mater. Struct.* **30** 015028
[46] Wu P, Yu T, Chen M and Hui D 2022 Effect of printing speed and part geometry on the self-deformation behaviors of 4D printed shape memory PLA using FDM *J. Manuf. Processes* **84** 1507–18
[47] Hosseinzadeh M, Ghoreishi M and Narooei K 2023 4D printing of shape memory polylactic acid beams: An experimental investigation into FDM additive manufacturing process parameters, mathematical modeling and optimization *J. Manuf. Process.* **85** 774–82
[48] Hoa S V and Cai X 2020 Twisted composite structures made by 4D printing method *Compos. Struct.* **238** 111883
[49] Guo J, Liu J, Wang Z, He X, Hu L, Tong L and Tang X 2017 A thermodynamics viscoelastic constitutive model for shape memory polymers *J. Alloys Compounds* **705** 146–55
[50] Ding Z, Yuan C, Peng X, Wang T, Qi H J and Dunn M L 2017 Direct 4D printing via active composite materials *Sci. Adv.* **3** e1602890
[51] Scalet G 2020 Two-way and multiple-way shape memory polymers for soft robotics: an overview *Actuators* **9** 10
[52] Wan X, He Y, Liu Y and Leng J 2022 4D printing of multiple shape memory polymer and nanocomposites with biocompatible, programmable and selectively actuated properties *Addit. Manuf.* **53** 102689
[53] Teoh J, An J, Chua C, Lv M, Krishnasamy V and Liu Y 2017 Hierarchically self-morphing structure through 4D printing *Virtual Phys. Prototyp.* **12** 61–68
[54] Zhou Y and Huang W M 2015 Shape memory effect in polymeric materials: mechanisms and optimization *Proc. IUTAM* **12** 83–92
[55] Withers P 2007 Residual stress and its role in failure *Rep. Progr. Phys.* **70** 2211
[56] Yin Z, Fan L and Wang T 2008 Experimental investigation of the viscoelastic deformation of PC, ABS and PC/ABS alloys *Mater. Lett.* **62** 2750–3
[57] Goo B, Hong C H and Park K 2020 4D printing using anisotropic thermal deformation of 3D-printed thermoplastic parts *Mater. Des.* **188** 108485
[58] Nezhad I S, Golzar M, Behravesh A H and Zare S 2022 Comprehensive study on shape shifting behaviors in FDM-based 4D printing of bilayer structures *Int. J. Adv. Manuf. Technol.* **120** 959–74
[59] Lee H M, Sung J, Ko B, Lee H, Park S, So H and Yoon G H 2021 Modeling and application of anisotropic hyperelasticity of PDMS polymers with surface patterns obtained by additive manufacturing technology *J. Mech. Behav. Biomed. Mater.* **118** 104412
[60] Menard K, Cassel B and Shelton C 2013 *Basics of Thermomechanical Analysis With tma 4000* (PerkinElmer, Inc)
[61] Noroozi R, Bodaghi M, Jafari H, Zolfagharian A and Fotouhi M 2020 Shape-adaptive metastructures with variable bandgap regions by 4D printing *Polymers* **12** 519
[62] Yu Y, Liu H, Qian K, Yang H, McGehee M, Gu J, Luo D, Yao L and Zhang Y J 2020 Material characterization and precise finite element analysis of fiber reinforced thermoplastic composites for 4D printing *Comput.-Aided Design.* **122** 102817